THE INFLUENCE OF THE CRUCIBLE AND THE COOLING RATE ON THE STRUCTURE OF GLASSES AND GLASS-CRYSTALLINE MATERIALS IN THE $CaO-Na_2O-P_2O_5-B_2O_3$ SYSTEM

Tina Tasheva

Department of Silicate Technology
University of Chemical Technology and Metallurgy
8 Kliment Ohridski Blvd., Sofia 1797, Bulgaria
E-mail: tina.tasheva@uctm.edu

Received 17 June 2025
Accepted 17 July 2025
DOI: 10.59957/jctm.v60.i5.2025.15

ABSTRACT

Batches with composition $47.2B_2O_3$-$24.98Na_2O$-$27.54CaO$-$0.27P_2O_5$ (mol %) were melted in porcelain and corundum crucibles by melt quenching and normal cooling rate techniques. As a result, four different materials were obtained. Powder X-ray diffraction analysis showed that the sample melt in a corundum crucible and melt-quenched was almost fully amorphous, whereas its slowly cooled analogue exhibited near-complete crystallization. Samples prepared in porcelain crucibles, regardless of cooling technique, had predominantly amorphous structures, but two different crystalline phases appeared when the melts were slowly cooled. Scanning electron microscopy revealed distinct microstructural differences between the slowly cooled samples from porcelain and corundum crucibles. Fourier-transform infrared and Raman spectroscopy identified BO_3 and BO_4 units as the main structural units, likely interconnected in pentaborate superstructural units. The influence of crucible material on crystallization behavior and phase formation was discussed.

Keywords: *Borate glasses, glass-ceramics, IR spectra, Raman spectra.*

INTRODUCTION

In recent decades, the intersection of materials science and medicine has given rise to a new generation of biofunctional materials designed to interact with living tissues in a controlled and beneficial manner. As the demand for improved healthcare solutions grows, driven by an aging population, rising chronic disease rates, and the increasing expectations for quality of life, so too does the need for advanced biomaterials capable of not only replacing damaged tissues, but also promoting their regeneration. Among the broad spectrum of materials developed for biomedical applications, bioactive ceramics have gained particular attention. These materials exhibit a unique combination of biocompatibility, structural integrity, and, most importantly, the ability to bond chemically with bone and, in some cases, soft tissue.

Bioactive ceramics are now widely used across various surgical disciplines [1, 2]. In orthopedics, they serve as bone graft substitutes and components of joint prostheses, in oral and maxillofacial surgery, they are employed for dental implants and facial reconstruction, in plastic and reconstructive surgery, they support the repair of craniofacial defects, while in vascular and otolaryngology (ENT) applications, they assist in tissue engineering and scaffold design.

Other widely used inorganic materials are bioactive glasses which have emerged as a distinct and promising class of materials due to their unique ability to bond with hard and soft tissues, as well as to stimulate cellular responses that support healing and regeneration. Bioactive glasses (BGs) are recognized for their high surface reactivity when exposed to physiological environments such as human plasma or phosphate-rich aqueous solutions [3 - 7].

Bioactive borate glasses (BBGs) have demonstrated significant potential across a range of biomedical applications due to their high dissolution rates and controllable release profiles [7 - 9]. Their rapid degradation and ability to stimulate tissue responses make them especially suitable for bone regeneration, where timely resorption and osteoconductivity are critical. BBGs have also been applied in wound healing, leveraging their angiogenic and antibacterial properties to accelerate tissue repair [8 - 13]. Moreover, their compositional flexibility allows for the incorporation of therapeutic ions (e.g., Sr^{2+}, Cu^{2+}, Zn^{2+}), enhancing biological functions such as vascularization, osteogenesis, and antimicrobial defense [8, 12, 14]. These diverse capabilities position BBGs as promising candidates for next-generation biomaterials in both hard and soft tissue engineering.

B_2O_3 is one of the known glass formers, and borate glasses have been extensively studied due to their properties. In these glasses, the ratio between BO_4 and BO_3 is modifier-dependent and changes with the type and concentration of modifier [15, 16]. The addition of network modifiers, the properties of borates frequently exhibit extrema at specific values of the network-modifier fraction, which is known as the borate anomaly, or boron oxide anomaly. When a network modifier is first introduced to B_2O_3, it primarily promotes the transformation of boron coordination from trigonal $BØ_3$ units to tetrahedral $BØ_4^-$ units, rather than immediately producing nonbridging oxygen atoms (NBOs). These NBOs typically appear only at higher concentrations of the modifier. The borate structures are commonly represented as $B^{(n)}$, where 'n' indicates the number of bridging oxygen atoms (Ø) that connect adjacent units [16 - 18].

The purpose of this investigation is to examine the structural characteristics glasses, within the B_2O_3-Na_2O-CaO-P_2O_5 system. The present study focuses on the synthesis conditions, specifically, the influence of the crucible material and cooling rate, and how these factors affect the borate network.

EXPERIMENTAL

Four different materials with the same composition $47.2B_2O_3$-$24.98Na_2O$-27.54CaO-$0.27P_2O_5$ (mol %) were obtained in porcelain and corundum crucibles and after different cooling rates. The raw materials used B_2O_3 (Alfa Aesar, 99 %), Na_2CO_3 (Alfa Aesar, 99.5 %), CaO (Alfa Aesar, 99.5 %), and H_2PO_4 (Alfa Aesar, 99.2 %) were homogenized in an agate mortar for 15 min. Four batches with the same composition were prepared: two of them were melted in porcelain crucibles and the other two in corundum crucibles at a temperature of 350°C for 20 min, after which the temperature was raised to 950°C for another 20 min. The melts were stirred several times during heating. One melt from each type of crucible was cooled using the melt-quenching technique: poured onto an aluminium plate and pressed to a thickness of 1 - 2 mm using a copper plate. The remaining melts were poured onto the plate but cooled gradually to room temperature. As a result, four different materials were obtained. Powder X-ray diffraction (XRD) patterns were recorded for the samples in the range of 5.3 to 80° 2θ, with a constant step size of 0.03° 2θ and a counting time of 52.5 sec per step, using a Bruker D8 Advance diffractometer (Germany) with Cu Kα radiation and a LynxEye detector. FT-IR spectra were recorded in the range of 2000 - 400 cm^{-1} using a Varian 600-IR FT-IR spectrometer. Samples for these measurements were prepared in the form of KBr pellets. The accuracy of the absorption maxima is ± 3 cm^{-1}. Raman Renishaw inVia microscope with Leica DM2700 M; Analysis' conditions: laser: 532 nm, integration time: 10 sec, laser power: 10mW, 3 accumulations. Photoelectron spectra were recorded using an ESCALAB MK II X-ray photoelectron spectrometer with a non-monochromatic Al X-ray source under vacuum better than 10^{-7} Pa, at a take-off angle of 45°, and with an overall instrumental resolution of 1 eV. Binding energies (BE) were determined using the C1s line (from adventitious carbon) as a reference at 285.0 eV. The accuracy of the measured binding energy is 0.2 eV. Surface concentrations of the constituent elements were calculated from the peak area after subtracting a Shirley-type background. SEM images were acquired using a JEOL JEM200CX at an accelerating voltage of 25 kV.

RESULTS AND DISCUSSION

The results obtained by X-ray powder diffraction are given in Figs. 1 - 4. The diffractograms of the samples melted in corundum and porcelain crucibles by melt-quenching technique are shown in Figs. 1 and 2 and those by slowly melted are shown in Figs. 3 and 4,

respectively. Samples 1 and 2 are characterized by well-defined amorphous halo but also some crystalline peaks appear. In Sample 1 (melted in corundum, melt-quenched, Fig. 1), these peaks are not well defined, while in Sample 2 (melted in porcelain, melt-quenched, Fig. 2), the peaks are of higher intensity. These peaks are related to the diffraction of the α-$CaNaPO_4$ phase (Ref. code 98-002-7957). Sample 3, melted in a corundum crucible, slowly cooled, is almost fully crystallized and characterized by the presence of two crystalline phases: AlP_3O_9 (Ref. code 98-000-0170) of 95.2 %, and $CaNa_3B_5O_{10}$ (Ref. code 98-006-1165) of 4.8 % (Fig. 3). Sample 4, melted in a porcelain crucible, and slowly cooled (Fig. 4), is also constituted by two crystalline phases: $CaNa_3B_5O_{10}$ (Ref. code 98-006-1165) - 84.4 %, and α-$CaNaPO_4$ (Ref. code. 98-002-7957 - 15.6 %. The use of a corundum crucible during melting introduces significant aluminum contamination, as evidenced by the formation of 95.2 % $AlPO_3$ in the diffraction pattern of the slowly cooled sample (Fig. 3). This result indicates the incorporation of alumina-derived Al^{3+} ions into the melt. The presence of aluminum also affects the glass-formation ability: in the melt-quenched sample, melted in a corundum crucible, the amorphous phase is well represented, and the growth of the α-$CaNaPO_4$ phase is restricted.

To determine the main structural units that make up the structure of the glasses, the IR spectra (Fig. 5) and the Raman spectra (Fig. 6) of the materials in the B_2O_3-Na_2O-CaO-P_2O_5 system were recorded. It is noteworthy that the IR spectra of the glasses melted in porcelain and corundum crucibles, melt-quenched, almost do not differ. The analysis of the spectra was made based on

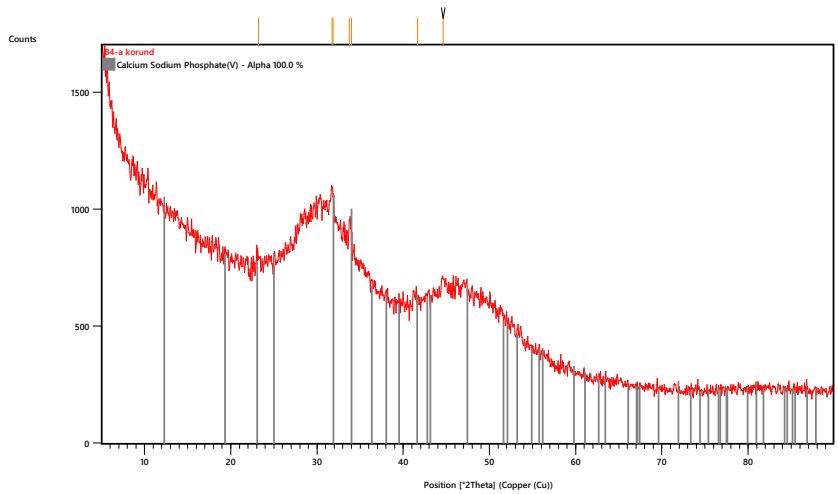

Fig. 1. XRD pattern of the sample, melted in a corundum crucible, melt-quenched.

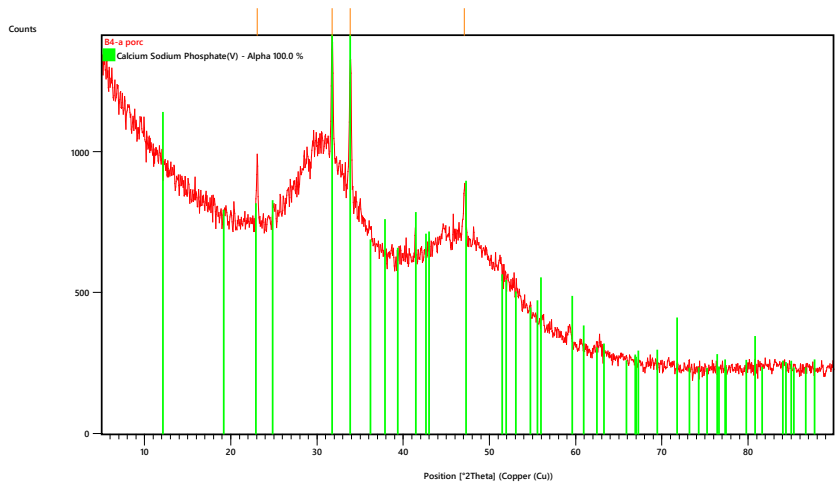

Fig. 2. XRD pattern of the sample, melted in a porcelain crucible, melt-quenched.

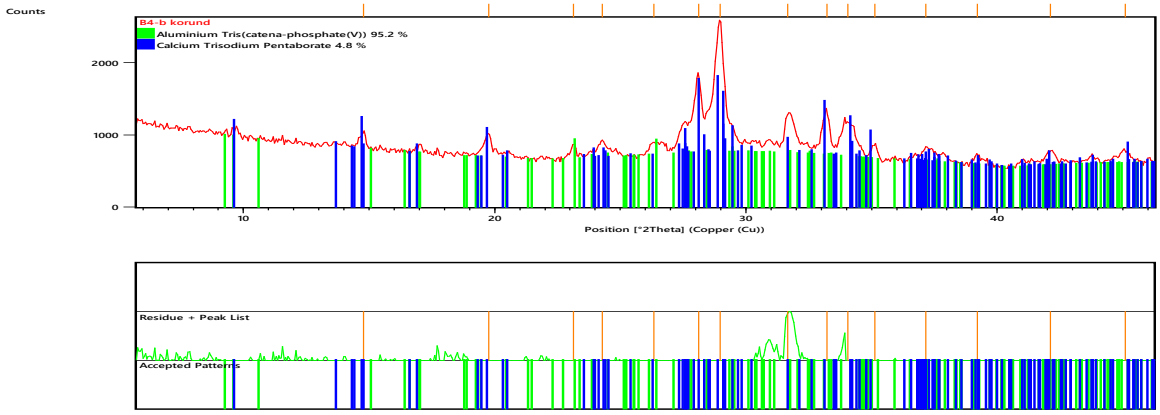

Fig. 3. XRD pattern of a sample, melted in a corundum crucible, slowly cooled.

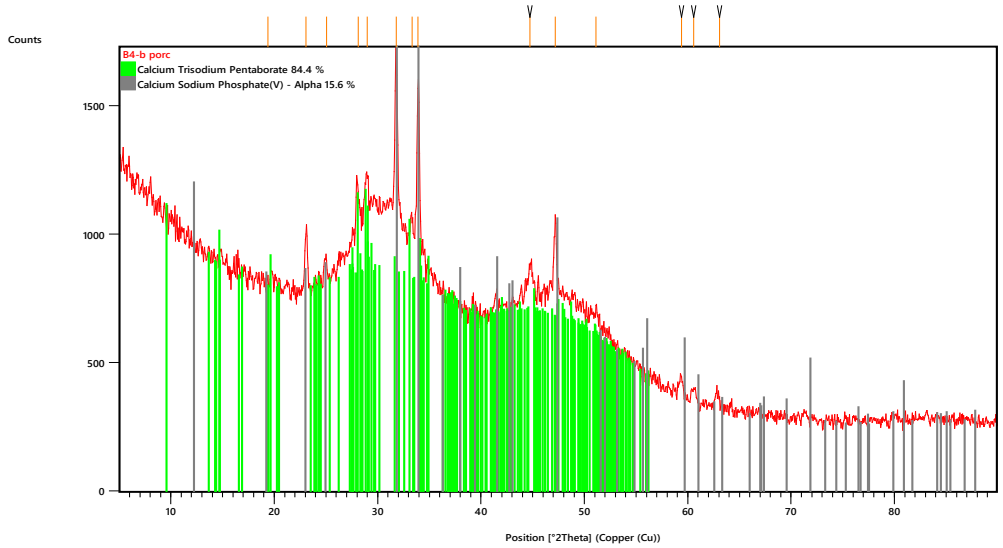

Fig. 4. XRD pattern of a sample, melted in a porcelain crucible, slowly cooled.

the characteristic vibrations of metal-oxygen units found in various binary and triple crystalline and amorphous materials with similar composition. The IR spectra of the samples obtained in porcelain and corundum crucibles are characterized by the following well-defined bands: 1408 cm^{-1}; 1250 - 1200 cm^{-1}; 1025 cm^{-1}; 942 cm^{-1}; 715 cm^{-1} and 569 cm^{-1}.

In the mid-infrared region (500 - 1650 cm^{-1}), three broad absorption envelopes are observed, corresponding to vibrations of the borate network-forming polyhedra [15, 18 - 20]. The asymmetric B-O stretching modes of tetrahedral borate units ($BØ_4^-$) dominate the 800 - 1200 cm^{-1} range. In contrast, the stretching vibrations of triangular borate species ($BØ_3$ and $BØ_2O^-$) appear at higher frequencies, typically between 1200 and 1650 cm^{-1}. Additionally, weaker bands occurring in the 550 - 800 cm^{-1} range are attributed to deformation modes of the network-forming units.

The bands recorded on the IR spectra of the glasses could be assigned as follows. The bands in the high-frequency region at 1408 cm^{-1} and 1250 - 1200 cm^{-1} are related to the B-O antisymmetric valence vibration of the BO_3 group and the B-O-B valence vibration of the BO_3 group. The absence of a band at 1380 cm^{-1} characteristic of the B-O valence vibration of the BO_3 group in a boroxol ring and the absence of a band in the 680 -

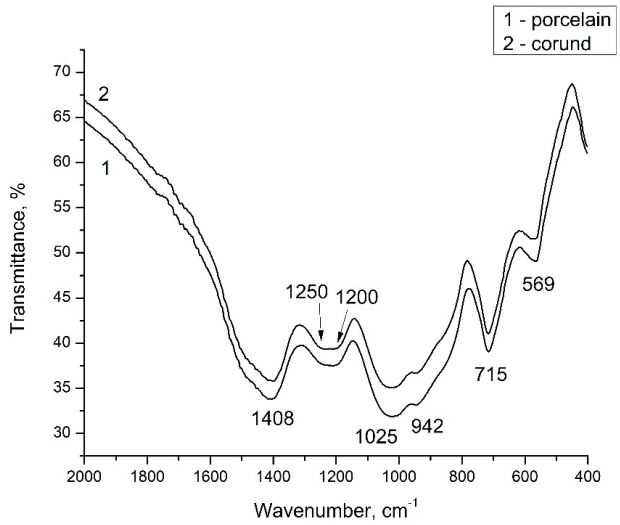

Fig. 5. FT-IR spectra of glass melted in porcelain (1) and corundum (2) crucible, melt-quenched.

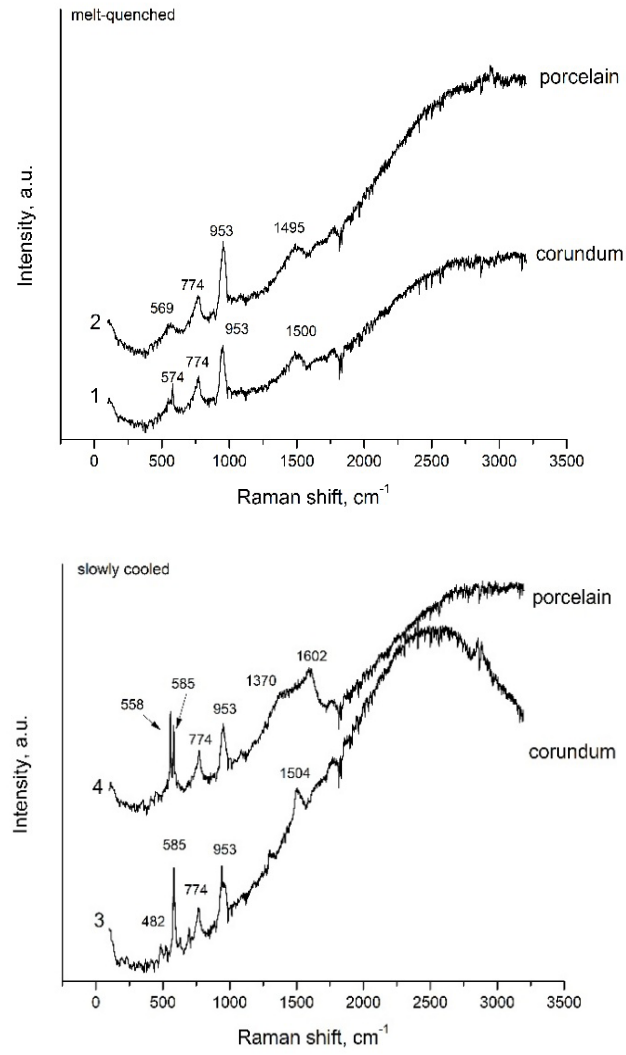

Fig. 6. Raman spectra of the samples: 1 - melted in corundum crucible, melt-quenched; 2 - melted in porcelain crucible, melt-quenched; 3 - melted in corundum crucible, slowly-cooled- melted in porcelain crucible, slowly-cooled.

670 cm^{-1} region excludes the formation of entirely boroxol rings and metaborate groups. The IR spectra of borates containing a tetrahedral BO_4 group are characterised by intense bands in the 1150 - 850 cm^{-1} region, which are observed in the spectra. The band at 1025 cm^{-1} and the one at 942 cm^{-1} could be assigned to the B-O valence oscillation of the BO_4 group in pentaborates.

The Raman spectra are characterised by several well-defined bands: at around 569 - 585 cm^{-1}, at 774 cm^{-1}, 963 cm^{-1}, around 1500 cm^{-1} and in case of Sample 4 two more bands at 1370 cm^{-1} and 1602 cm^{-1} appears (Fig. 6). The bands at 774 cm^{-1} and 953 cm^{-1} remain unchanged in both position and intensity across all sample spectra. The band around 570 - 585 cm^{-1} increases its intensity when compare melt-quenched and slowly cooled samples and in the spectra of the Sample 4 (melt in porcelain crucible and slowly cooled down) a doublet appears at 558 cm^{-1} and 585 cm^{-1}. The high frequency range of this spectra is also different than the other sample's spectra - new bands at 1370 cm^{-1} and 1602 cm^{-1} are observed (Fig. 6 b). A low intensity peak appears in the spectra of the in Sample 3 (melt in corundum crucible and slowly cooled down) at 482 cm^{-1} (Fig. 6 b).

The appearance of the band at 482 cm^{-1} could be related with the Al-O vibrations of AlO_6 structural units caused by the contamination of the crucible [21]. The band at 774 cm^{-1} could be explained by the bending vibrations $\delta(A_2)$ of trigonal BO_3 unit and the stretching vibration of tetragonal BO_4 unit of pyroborate unit, the band at 953 cm^{-1} is also related by the vibrations of pentaborate units. The band around 1500 cm^{-1} corresponded to BO_2O^- triangle either linked to BO_4^- or to another triangular units [15].

Figs. 7 and 8 show the results obtained by X-ray photoelectric spectroscopy (XPS). 1s, Ca2p, P2p, Na1s, O1s connecting energies are registered. XPS analysis shows that all components in the glasses are in an oxidative state. The only difference between the two samples is the amount of bridging and non-bridging

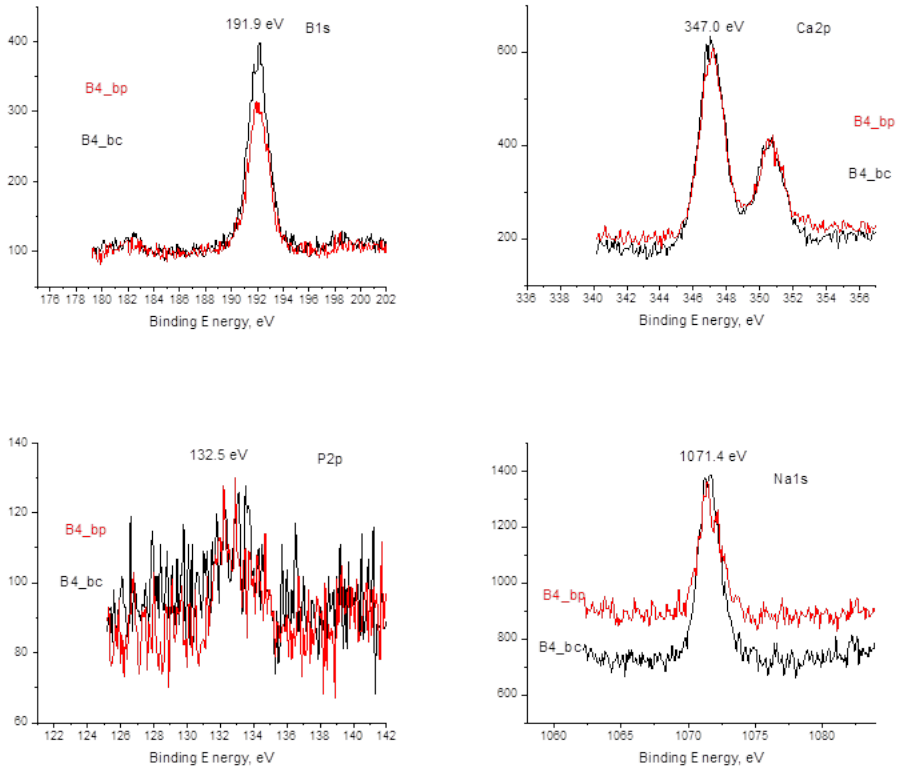

Fig. 7. XPS spectra of glass molten in porcelain (red) and corundum (black) crucibles, melt-quenched.

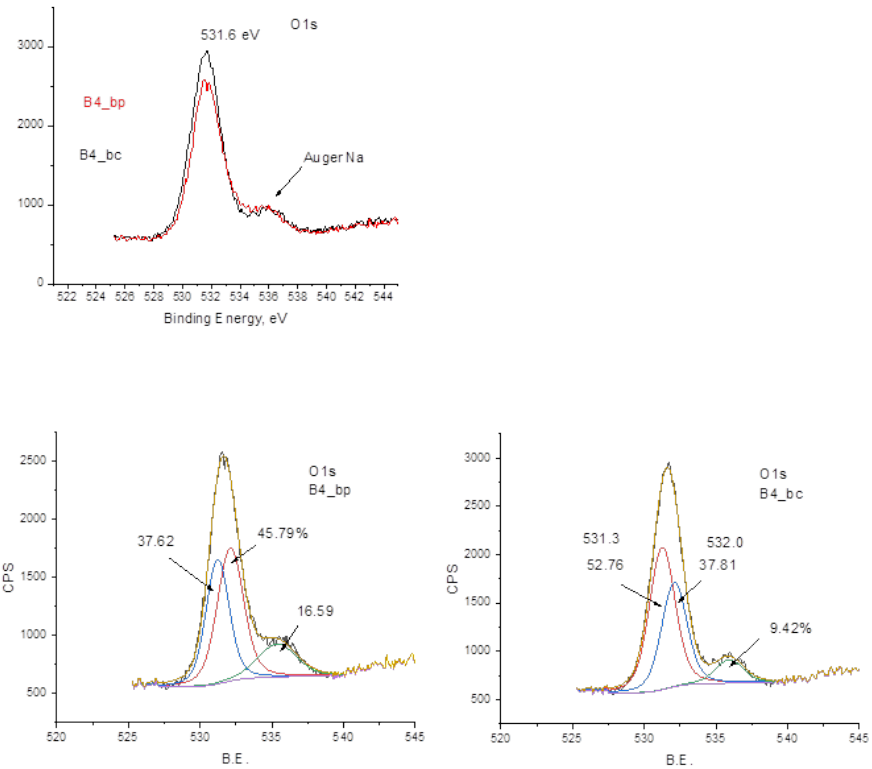

Fig. 8. XPS spectra of (a) glass melted in porcelain (red) and corundum (black) crucibles, melt-quenched and their deconvoluted spectra (b).

oxygen (Fig. 8). The different amount of P could explain this difference in the two samples.

Figs. 9 and 10 show the SEM images of the slowly cooled porcelain and corundum crucible melts, respectively. It is noteworthy that there is a significant difference in morphology between the obtained materials depending on the method of synthesis.

From the analyses made, it could be noted that the influence of the crucible has a significant role, as well as the rate of cooling. The results obtained show that amorphous material is observed in both types of crucibles when the melts are cooled rapidly, as well as when the melt is slow cooled in the porcelain crucible while in the case of the porcelain crucible, the phase is more pronounced. This could be explained by the fact that a certain amount of Al from the crucible entered the melt and led to the stabilization of the amorphous phase. Unlike the sharply cooled melt of the corundum crucible, in the smoothly cooled one, crystallization is observed and the amorphous phase is not noticeable. It is also noteworthy that only in the smoothly cooled melt of the corundum crucible the AlP_3O_9 phase is formed and thus Al manages to bind to the entire amount of phosphorus and this prevents the formation of $CaNaPO_4$.

The traditionally used hydroxyapatite, $Ca_{10}(PO_4)_6(OH)_2$, has the lowest solubility among calcium phosphates. In cases of regenerative treatment approaches of joint tissue, bioredigestible phases are preferred materials with

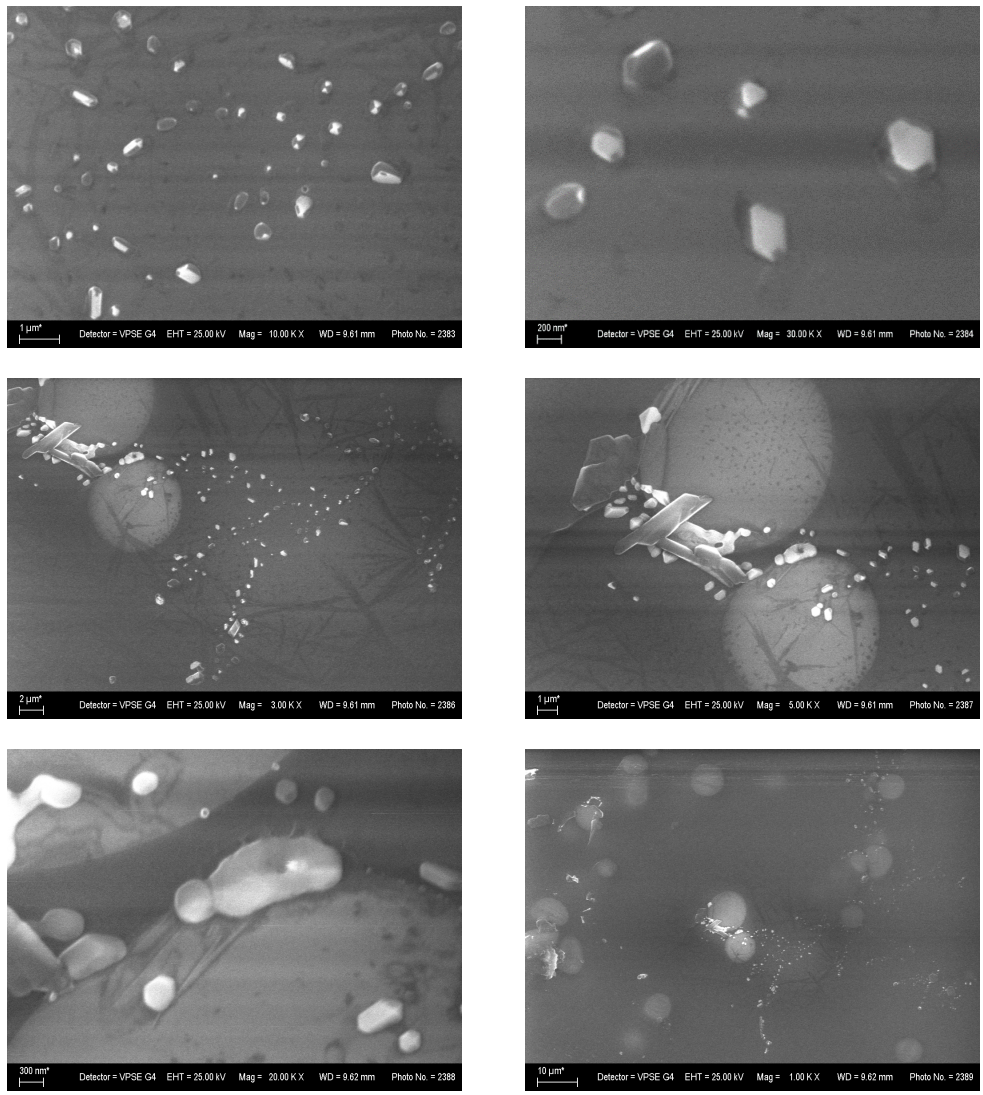

Fig. 9. SEM images of a slowly cooled sample, melted in a porcelain crucible.

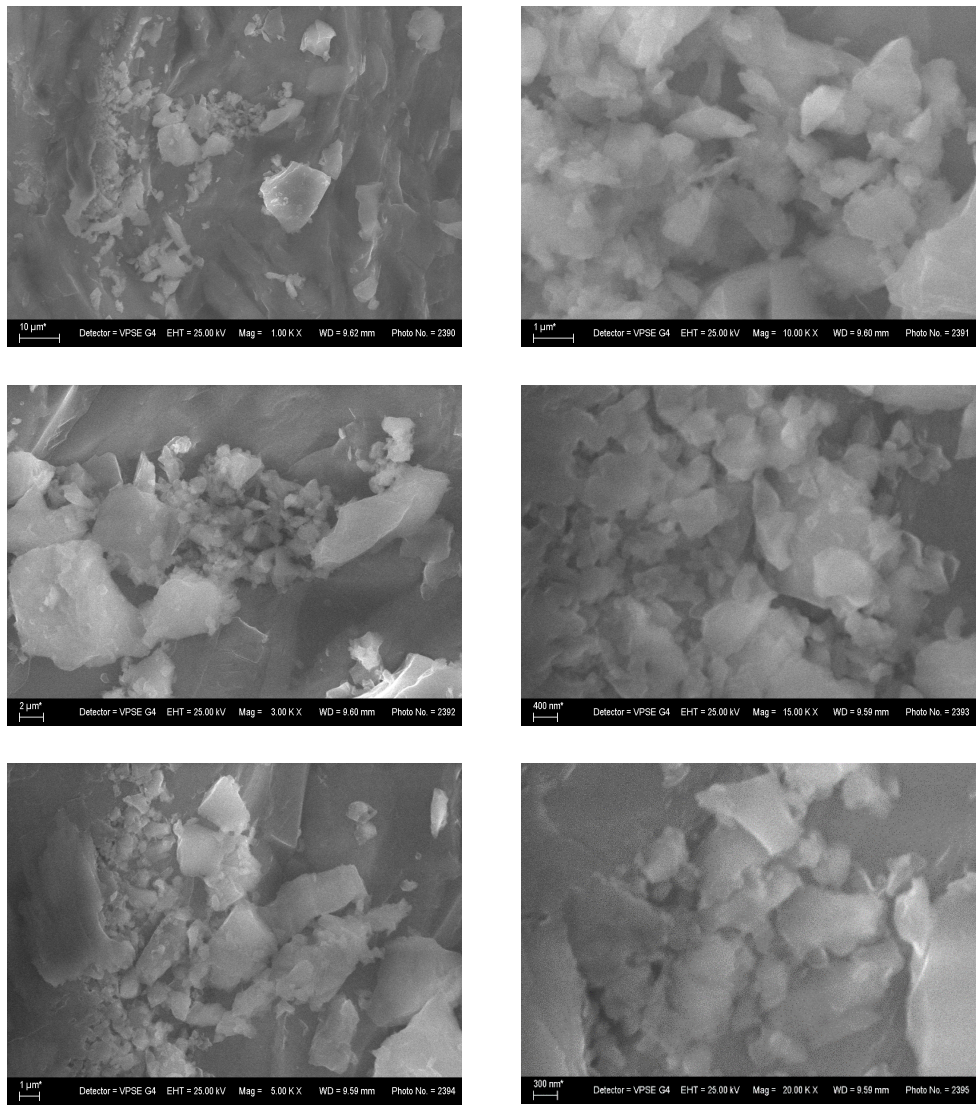

Fig. 10. SEM Images of a slowly cooled sample, melted in a corundum crucible.

higher restorability, including sodium renanite $CaNaPO_4$ [6]. This phase is observed in the greatest quantity in the materials obtained in the porcelain crucible, only slightly in the sharply cooled corundum glass and is not observed in the smoothly cooled corundum crucible melt. On the other hand, the formed AlP_3O_9 phase is of interest in the field of integrated circuits.

CONCLUSIONS

Four different materials with composition $47.2B_2O_3$-$24.98Na_2O$-27.54CaO-$0.27P_2O_5$ (mol %) were obtained due to the different cooling rates and the crucible type: 1) melt-quenched from porcelain crucible: glass with a small amount of crystalline phase composed of α - calcium sodium phosphate $CaNaPO_4$ (renanite); 2) melt-quenched from corundum crucible: glass with a negligible amount of crystalline phase composed of α - calcium sodium phosphate $CaNaPO_4$ (renanite); 3) slowly cooled melt from porcelain crucible: crystal phase glass composed of calcium trisodium pentaborate $CaNa_3BO_{10}$ (84.4 %) and α - calcium sodium phosphate $CaNaPO_4$ (renanite) and 4) slowly cooled melt from corundum crucible: crystalline material composed of Aluminium Tris(caneta-phosphate (V)) AlP_3O_9 (95.2 %) and calcium trisodium pentaborate $CaNa_3BO_{10}$ (4.8%). This suggests that a significant amount of Al from the crucible reacted with the melt and played the role of

network former in the melt-quenched samples melted in a corundum crucible, with almost no crystalline phase observed on the XRD pattern. Furthermore, Al has formed a crystalline phase with P in the slowly cooled sample melted in a corundum crucible. The results of the FT - IR and Raman spectra show that the main structural units constituting the borate network are BO_3 and BO_4^- structural units, connected in a pentaborate structural unit.

Acknowledgements

This research is supported by the Bulgarian National Science Fund, Competition for financial support for projects of junior basic researchers and postdocs - 2022 under grant КП-06-М69/6. The Raman spectroscopy was performed as part of contract №: BG-RRP-2.004-0002-C01, project name: BiOrgaMCT, Procedure BG-RRP-2.004 „Establishing of a network of research higher education institutions in Bulgaria", funded by Bulgarian National Recovery and Resilience Plan.

Authors' contributions*: T.T.: Conceptualization, methodology, data curation, writing: original draft preparation, review and editing, visualization, funding acquisition.*

REFERENCES

1. B.J. McEntire, B.S. Bal, M.N. Rahaman, J. Chevalier, G. Pezzotti, Ceramics and ceramic coatings in orthopaedics, J. Eur. Ceram. Soc., 35, 16, 2015, 4327-4369.
2. An Introduction to Bioceramics, Second Edition, Editor L. Hench, 2013, Imperial College Press.
3. A.M. Brokesh, A.K. Gaharwar, Inorganic Biomaterials for Regenerative Medicine, ACS Appl. Mater. Interfaces, 12, 5, 2020, 5319-5344. https://dx.doi.org/10.1021/acsami.9b17801
4. Q.Z. Chen, I.D. Thompson, A.R. Boccaccinia, 45S5 Bioglasss-derived glass-ceramic scaffolds for bone tissue engineering, Biomaterials 27, 2006, 2414-2425. doi:10.1016/j.biomaterials.2005.11.025
5. L.L. Hench, J.R. Jones, Bioactive Glasses: Frontiers and Challenges, Front Bioeng Biotechnol 30, 3, 2015, 194. doi:10.3389/fbioe.2015.00194
6. I. Negut, C. Ristoscu, Bioactive Glasses for Soft and Hard Tissue Healing Applications-A Short Review, Appl. Sci., 13, 2023, 6151. https://doi.org/10.3390/app13106151
7. D. Ege, K. Zheng, A.R. Boccaccini, Review: Borate Bioactive Glasses (BBG): Bone Regeneration, Wound Healing Applications, and Future Directions, ACS Appl. Bio Mater. 5, 8, 2022, 3608-3622, https://doi.org/10.1021/acsabm.2c00384
8. S. Fakher, D. Westenberg, Borate-based bioactive glasses properties: Clinical and biomedical applications, Ceram. Internat., 50, 2024, 52190-52204. https://doi.org/10.1016/j.ceramint.2024.10.194
9. X. Liu, M.N. Rahaman, D. Day, Conversion of melt-derived microfibrous borate (13-93B3) and silicate (45S5) bioactive glass in a simulated body fluid, J. Mat. Sci.: Mater. Med., 24, 3, 2013, 583-595.
10. L. Bi, M.N. Rahaman, D.E. Day, Z.Brown, C.Samujh, X. Liu, A. Mohammadkhah, V. Dusevich, J. David Eick, L.F. Bonewald, Effect of bioactive borate glass microstructure on bone regeneration, angiogenesis, and hydroxyapatite conversion in a rat calvarial defect model, Acta Biomaterialia, 9, 2013, 8015-8026. http://dx.doi.org/10.1016/j.actbio.2013.04.043
11. L. Bi, B. Zobell, X. Liu, M.N. Rahaman, L.F. Bonewald, Healing of critical-size segmental defects in rat femora using strong porous bioactive glass scaffolds, Mater. Sci. Eng. C., 42, 2014, 816-824.
12. G. Lopes da Silva, I.F. Rodrigues, S.S.S. Pereira, G.M.G. Fontoura, A.S. Reis, F. Pedrochi, A. Steimacher, Bioactive antibacterial borate glass and glass-ceramics, J. Non-Cryst. Solids, 595, 2022, 121829
13. S. Kargozar, F.Baino, S. Hamzehlou, R.G. Hill, M.Mozafari, Bioactive Glasses: Sprouting Angiogenesis in Tissue Engineering, Trends in Biotechnology, 36, 4, 2018, 430-444. https://doi.org/10.1016/j.tibtech.2017.12.003
14. O.D. Abodunrin, K. El Mabrouk, M. Bricha, A review on bioactive glasses (BBG): effect of doping elements, degradation, and applications, J. Mater. Chem. B, 11, 2023, 955-973. DOI:10.1039/d2tb02505a
15. T. Tasheva, G. Valova, FT-IR and Raman spectroscopy of ZnO and MgO containing glasses in the B_2O_3/Na_2O/CaO/P_2O_5 system, J. Chem. Technol. Metall., 59, 6, 2024, 1391-1398. DOI: 10.59957/jctm.v59.i6.2024.14

16. A.A. Ali, Y.S. Rammah, R. El-Mallawany, D. Souri, FTIR and UV spectra of pentaternary borate glasses, Measurement 105, 2017, 72-22. http://dx.doi.org/10.1016/j.measurement.2017.04.010
17. A.C. Wright, My Borate Life: An Enigmatic Journey, Int. J. Appl. Glass Sci., 6, 1, 2015, 45-63.
18. B. Topper, E.M. Tsekrekas, L. Greiner, R.E. Youngman, E.I. Kamitsos, D. Möncke, The dual role of bismuth in Li_2O-Bi_2O_3-B_2O_3 glasses along the orthoborate join, J. Am. Ceram. Soc., 105, 2022, 7302-7320. https://doi.org/10.1111/jace.18699
19. A. Yoleva, T. Tasheva, D. Djambazov, A. Batsova, Development of multicomponent glasses for application as a glazing layer on dental zirconia, Int. J. Appl. Glass Sci., 2025, 16:e16684. https://doi.org/10.1111/ijag.16684
20. E. Kamitsos, Infrared spectroscopy and silicate glass structure, Phys. Chem. Glasses, 44, 2, 2003, 79-87.
21. A. Boumaza, L. Favaro, J. Lédion, G. Sattonnay, J.B. Brubach, P. Berthet, A.M. Huntz, P. Roy, R. Tétot, Transition alumina phases induced by heat treatment of boehmite: An X-ray diffraction and infrared spectroscopy study, J. Solid State Chem., 182, 2009, 1171-1176.